Helical domain walls in constricted cylindrical NiFe nanowires

Tran, M.; Chandra Sekhar, M.; Liew, H. F.; Han, G. C.; Purnama, Indra; Lew, Wen Siang

2012

Chandra, S. M., Liew, H. F., Purnama, I., Lew, W. S., Tran, M., & Han, G. C. (2012). Helical domain walls in constricted cylindrical NiFe nanowires. Applied Physics Letters, 101(15), 152406-.

https://hdl.handle.net/10356/95311

https://doi.org/10.1063/1.4758469

AIP | Applied Physics Letters

Helical domain walls in constricted cylindrical NiFe nanowires

M. Chandra Sekhar, H. F. Liew, I. Purnama, W. S. Lew, M. Tran et al.

Citation: Appl. Phys. Lett. **101**, 152406 (2012); doi: 10.1063/1.4758469
View online: http://dx.doi.org/10.1063/1.4758469
View Table of Contents: http://apl.aip.org/resource/1/APPLAB/v101/i15
Published by the American Institute of Physics.

Related Articles

Joule heating and current-induced domain wall motion
J. Appl. Phys. 112, 103922 (2012)

Application of local transverse fields for domain wall control in ferromagnetic nanowire arrays
Appl. Phys. Lett. 101, 192402 (2012)

Microwave assisted resonant domain wall nucleation in permalloy nanowires
Appl. Phys. Lett. 101, 172406 (2012)

Generation and storage of 360° domain walls in planar magnetic nanowires
J. Appl. Phys. 112, 083903 (2012)

Interplay between intrinsic and stacking-fault magnetic domains in bi-layered manganites
Appl. Phys. Lett. 101, 132402 (2012)

Additional information on Appl. Phys. Lett.

Journal Homepage: http://apl.aip.org/
Journal Information: http://apl.aip.org/about/about_the_journal
Top downloads: http://apl.aip.org/features/most_downloaded
Information for Authors: http://apl.aip.org/authors

ADVERTISEMENT

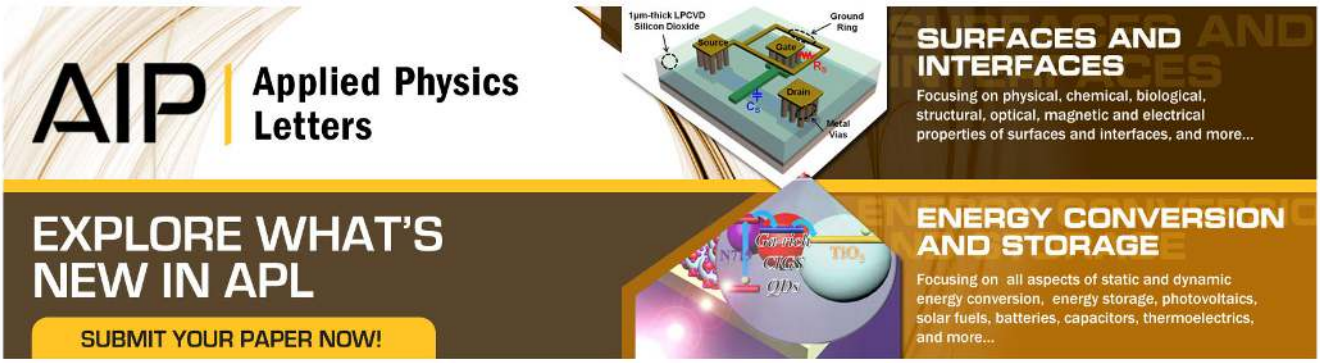

Helical domain walls in constricted cylindrical NiFe nanowires

M. Chandra Sekhar,[1] H. F. Liew,[1] I. Purnama,[1] W. S. Lew,[1,a)] M. Tran,[2] and G. C. Han[2]
[1]*School of Physical and Mathematical Sciences, Nanyang Technological University, 21 Nanyang Link, Singapore 637371*
[2]*Data Storage Institute, Agency of Science, Technology and Research (A*STAR), DSI Building, 5 Engineering Drive 1, Singapore 117608*

(Received 15 July 2012; accepted 25 September 2012; published online 11 October 2012)

Reducing the magnetic shape anisotropy of a cylindrical NiFe nanowire allows the formation of two vortices with opposite chirality at the two ends. At relatively low aspect ratio these two vortices are connected via a gradual rotation of the magnetization over a short region, which forms a three-dimensional helical domain wall. Micromagnetic simulations reveal that it is possible to control the number of helical domain walls in the cylindrical nanowire by geometrical constrictions engineering. A technique to create constricted $Ni_{95}Fe_5/Ni_{87}Fe_{13}$ multilayered nanowires is demonstrated, and magnetic force microscopy imaging was carried out to confirm the prediction of simulated helical domain walls. © *2012 American Institute of Physics*. [http://dx.doi.org/10.1063/1.4758469]

Magnetic domain walls (DWs) in planar and cylindrical ferromagnetic nanowires have received great interest due to their potential applications in magnetic logic and solid state memories.[1,2] Two types of DWs are generally found in a cylindrical magnetic nanowire depending on the nanowire diameter.[3,4] For diameters less than 50 nm, a transverse DW, which magnetization at the center of the wall is directed perpendicularly to the wire axis, is considered a stable configuration. When the diameter exceeds 50 nm, a vortex DW, is found to be more stable. Literature on the transverse DWs in cylindrical nanowires is relatively more established,[5–7] partly because the magnetization in low dimensional cylindrical nanowire is strictly confined along the nanowire long axis, and the magnetization and domain wall properties are very similar to those found in planar nanowires. However, as the diameter of the cylindrical magnetic nanowire increases, the shape anisotropy becomes a dominant term in the equation governing the magnetization equilibrium.[8–11] In the case of a soft magnetic material, e.g., permalloy, the magnetization equilibrium position is then essentially determined by the interplay between the shape anisotropy and the exchange interaction. The magnetization is therefore expected to curl from the end and gradually extend to the inner part along the cylindrical nanowire, forming a three-dimensional vortex magnetization with a clockwise or anti-clockwise orientation at each end. Further reducing the shape anisotropy can enhance the propagation of both vortices towards the center of the nanowire. If the geometry of the nanowire allows the two vortices to meet, a three-dimensional domain wall with helical magnetization is expected to form at the transition region.

In this letter, we use micromagnetic simulations to predict the existence of the above-mentioned three-dimensional helical DW and to determine which parameters allow its creation. To experimentally confirm our simulations, cylindrical NiFe nanowires with geometrical constrictions were fabricated using a combination of template-assisted electrodeposition and differential etching techniques. Magnetic force microscopy (MFM) measurements were performed on the constricted cylindrical NiFe nanowire to confirm the existence of the DW.

Three-dimensional micromagnetic simulations were carried out by using the OOMMF package.[12] The chosen unit cell size for all simulations is 10 nm × 5 nm × 5 nm. Shown in Figure 1(a) are the simulated magnetization configurations

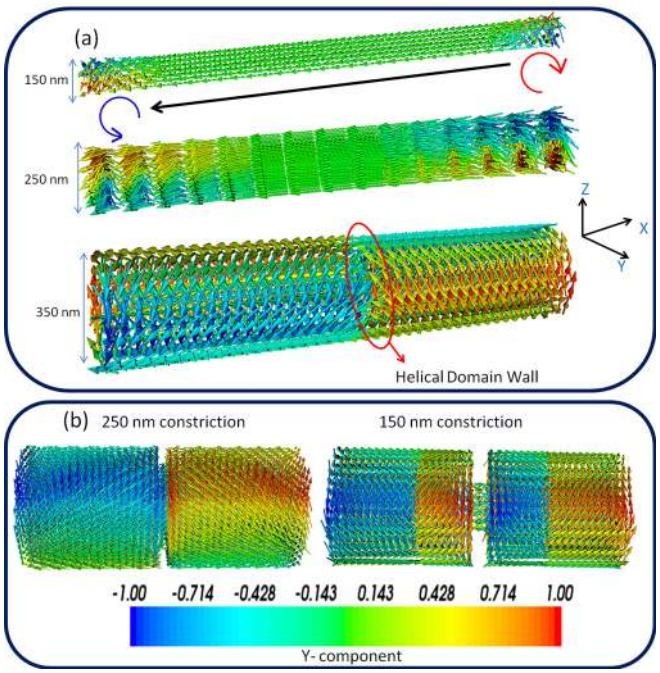

FIG. 1. (a) Simulated magnetization configuration of non-constricted cylindrical NiFe nanowires with diameters 150 nm, 250 nm, and 350 nm at remanent state. Three-dimensional vortex magnetization with clockwise or anticlockwise orientation is present at the ends of the nanowire, while most of the inner part is dominated with magnetization that aligns parallel to the nanowire long axis. When the diameter of the cylindrical nanowire increases, the two vortices gradually extends towards the center of the nanowire and eventually they are connected *via* a helical domain wall. (b) Simulated magnetization configuration of constricted cylindrical NiFe nanowires with a diameter of 350 nm at remanent state; the constriction dimensions are 250 nm and 150 nm.

a)Author to whom correspondence should be addressed. Electronic mail: wensiang@ntu.edu.sg.

of 3-μm-long NiFe nanowires at equilibrium for diameters 150 nm, 250 nm, and 350 nm. For a nanowire with a 150 nm diameter, the magnetization at the center region of the nanowire is aligned along the long axis because of the dominant shape anisotropy. However, at the two ends of the nanowire, the long axis shape anisotropy influence is reduced, and the magnetization is allowed to curl following the cylindrical shape of the nanowire. The magnetization curls in clockwise or anti-clockwise orientation at each end. As the nanowire diameter is increased to 250 nm, the long axis anisotropy is further reduced, and the magnetization curling is extended towards the center of the nanowire, forming two distinct vortices. When the diameter is further increased to 350 nm, the shape anisotropy energy completely dominates over the exchange energy, further extending the two vortices towards the center of the nanowire. Connection between these two vortices is completed *via* a gradual rotation of the magnetization at the center of the nanowire; thus, the transition region forms a helical DW. The simulation results confirm the intuition of the existence of a helical DW in cylindrical nanowires.

To control the number of helical domain walls present in the nanowire, we chose to introduce the constrictions along the nanowire. Introducing geometrical constrictions to the nanowire can lead to changes in the magnetization configuration. Shown in Figure 1(b) are simulated magnetization configurations of a 2-μm-long constricted cylindrical NiFe nanowire of 350 nm diameter, with a constriction at the center. When the constriction diameter is 250 nm, the simulated magnetization configuration is almost identical to that of the non-constricted nanowire. However, when the constriction diameter is decreased to 150 nm, additional DWs are found to be created within the structure on both sides of the constriction. This is due to the interaction between the longitudinal magnetization in the constriction segment and the transverse vortex magnetization in the larger diameter segment. For every n constrictions created in the nanowire $(n+1)$ DWs are present in the nanowire structure. The number of DWs is directly related to the number of the constrictions in the nanowire, while the distance between the DWs can be controlled by varying the length of the nanowire and the constriction segment.

Shown in Figure 2 is the calculated magnetic volume pole (Q) of a 350 nm diameter nanowire as a function of the position along its long axis. The magnetic volume pole is obtained by finding the divergence of the magnetization in the nanowire ($Q = -\nabla \bullet \vec{M}$). The plot reveals that negative and positive magnetic poles are present along the nanowire, and the crossover occurs at the center of the nanowire. The magnetic volume pole resembles the magnetic charge.[13] The magnetic charge variation along the long axis of the nanowire indicates that the two vortices of different chirality present in the nanowire can be identified by the polarity of the magnetic volume pole. Cross sectional views of the simulated magnetization configurations, from left to right along the nanowire, are shown above the plot. It shows that along the length of the nanowire the vortex cores of the clockwise and anti-clockwise orientations are slightly offset from the center of the nanowire long axis. The vortex core offset causes an imbalance of magnetization equilibrium, thus generating net magnetic charges at different positions. Consequently, the clockwise vortex configuration possesses a net positive magnetic charge whereas the anti-clockwise vortex configuration possesses a net negative magnetic charge. The transition between the two vortices is marked by the crossover from negative charge to positive charge, which has a length of ~100 nm. Within the transition region the magnitude of the magnetic charges increases abruptly before dropping to zero at the center. As we move from left to right along the long axis, the abrupt increase of the charge magnitude at "b" and "d" in Figure 2 is due to the onset of the annihilation of the anti-clockwise and clockwise vortex cores, respectively, causing a surge of the magnetization with similar orientation. At the center ("c" in the Figure 2), vortex core completely got annihilated which leads to the absence of the clockwise and anti-clockwise vortices resulting the average magnetization to be zero. This fulfills the minimum energy requirement of the magnetic system. The described three-dimensional magnetization configuration is almost mirroring one another at the center of the cylindrical nanowire.

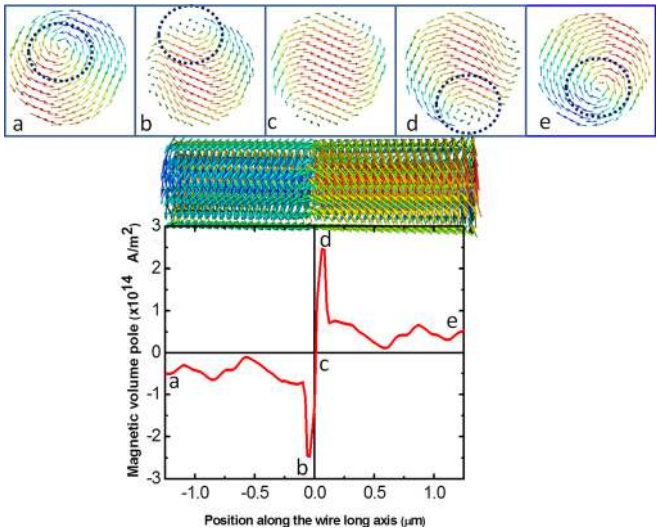

FIG. 2. The calculated magnetic volume pole as a function of the position along the long axis of the nanowire of 350 nm diameter. The magnetic volume pole value is obtained by taking the divergence of the magnetization. It is a representation of the magnetic charge present along the nanowire, and the pole sign indicates the chirality of the vortices formed. The transition region between the two peaks represents the helical domain wall. Also shown are the snapshot images of cross-sectional magnetization at various positions from left edge to right edge along the long axis of the nanwoire. The blue circle is the guideline for the vortex cores. The cross-sectional images are tagged with symbols (a)–(e) to represent the corresponding magnetic charge variations in the plot.

In order to confirm the simulation results, we have fabricated constricted cylindrical NiFe nanowire by a combination of template-assisted electrodeposition and differential etching techniques.[14] By applying electrical potential to a three-electrode cell, metal ions are driven into a nanoporous template, and material is deposited to form the desired metal nanowires. The applied potential strength and electrodeposition conditions are the key factors in determining the composition of the metal nanowires.[15–19] The chosen nanoporous template was an anodized aluminum oxide (AAO) (Anodisc 13, Whatman), and its backside was deposited with a 200 nm aluminium layer as electrical contact. The template was immersed in a 40 ml electrolyte bath, which is composed of

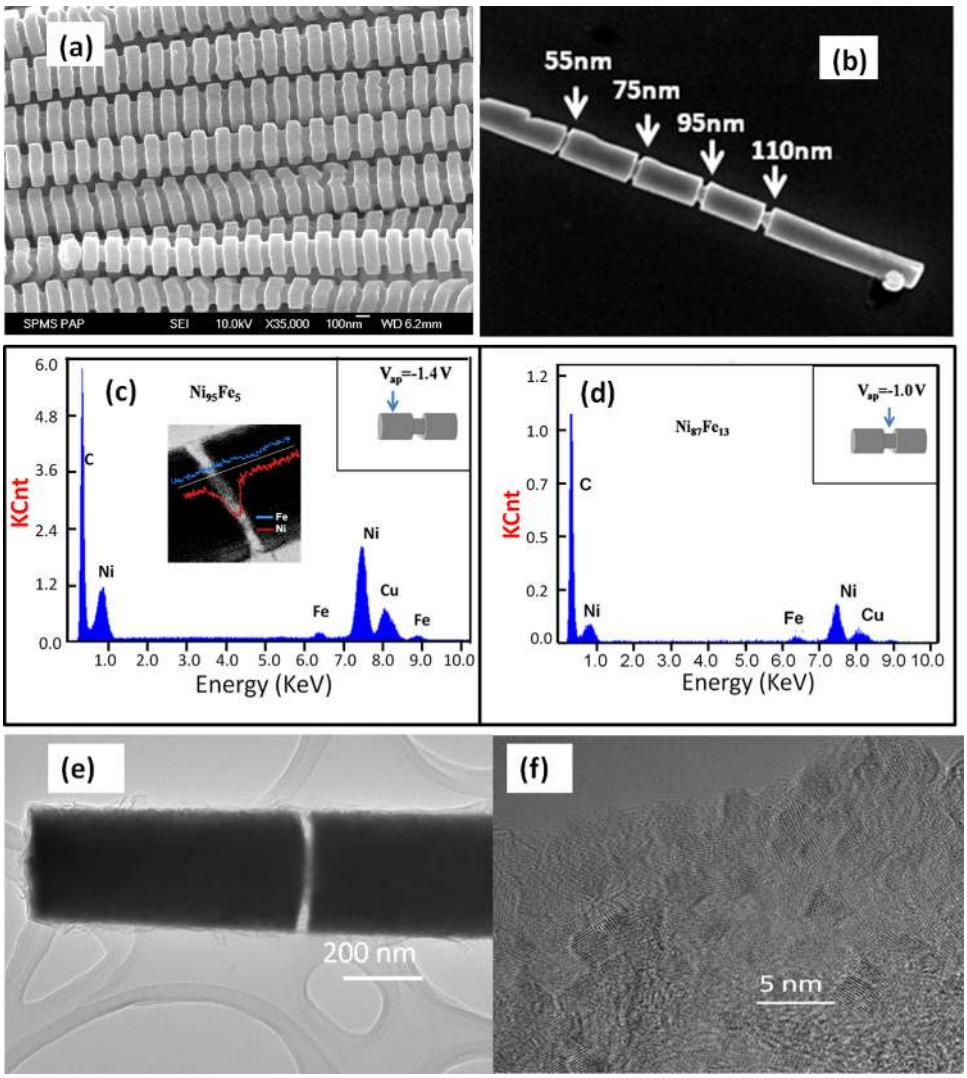

FIG. 3. (a) SEM image of constricted $Ni_{95}Fe_5$ ($l = 125$ nm, $Ø = 350$ nm)/$Ni_{87}Fe_{13}$ ($l = 50$ nm, $Ø = 250$ nm) nanowires. (b) A free standing individual strand of constricted $Ni_{95}Fe_5/Ni_{87}Fe_{13}$ nanowire with different dimension of constriction. (c), (d) EDX measurements of the Ni_xFe_{1-x} nanowire deposited at applied potentials of -1.4 V and -1.0 V. The composition is determined to be $Ni_{95}Fe_5$ and $Ni_{87}Fe_{13}$. Inset shows EDX elemental line scanning of Ni and Fe elements (Ni red, Fe blue) along the multilayered $Ni_{95}Fe_5$ and $Ni_{87}Fe_{13}$nanowires. (e) TEM image of a constricted $Ni_{95}Fe_5/Ni_{87}Fe_{13}$ nanowire. (f) Surface analysis morphology at the tip of the nanowire. The results indicate that the nanowire is polycrystalline with an alternate segment of $Ni_{95}Fe_5$ and $Ni_{87}Fe_{13}$.

0.5 M nickel sulfate, 0.01 M iron sulfate, and 0.5 M boric acid (pH = 4). During the Ni_xFe_{1-x} nanowires growth at a bath temperature 40 °C, the deposition potential was alternately switched between a high potential ($V_H = -1.4$ V), respectively, a low potential ($V_L = -1.0$ V) in a square waveform. The value of the electrical potential resulted in alternating layers of Ni_xFe_{1-x} and Ni_yFe_{1-y}, respectively, which relative thickness depend on the duration of each plateau. After the growth, the nanowires were released by dissolving the AAO template in 3 M NaOH, assisted by ultrasonic agitation. The multilayered $Ni_xFe_{1-x}/Ni_yFe_{1-y}$ nanowires were then thoroughly cleaned with deionized water before being selectively etched by 1% HNO_3 in order to fabricate the constrictions in the Ni_yFe_{1-y} layers.

Figure 3(a) shows SEM image of the etched nanowires, which has a modulation of diameter due to the different etching rate between the layers. The etch rate for the Ni_yFe_{1-y} layer is about 5 nm/s while that of Ni_xFe_{1-x} is negligibly small. Energy dispersive x-ray (EDX) scanning measurements were performed to confirm the relative composition of the layers. The measurements reveal that the compositions are x = 95% and y = 87% resulting in $Ni_{95}Fe_5$ and $Ni_{87}Fe_{13}$ in the segments deposited at V_H and V_L, respectively, as shown in Figures 3(c) and 3(d). During the nanowires deposition, the reduction process is in favor of Ni^{2+} as the potential difference is increased, giving Ni-rich layers when V_H is applied. EDX line scanning was performed across the nanowires, and the analysis (inset of Figure 3(c)) shows obvious decrease of Ni concentration at the $Ni_{87}Fe_{13}$ segment while the fluctuations of the Fe element at both segments are negligibly small. The reduced diameter $Ni_{87}Fe_{13}$ structure is considered the constriction region of the nanowire, and its shape and size along the nanowires are well defined and uniform. Figure 3(b) shows the constricted structure of the $Ni_{95}Fe_5/Ni_{87}Fe_{13}$ cylindrical nanowires that can be well modulated by changing the growth rate and the etching time of the $Ni_{95}Fe_5$ and $Ni_{87}Fe_{13}$ segments. Transmission electron microscopy (TEM) was also performed to visualize the nanowire surface morphology, as shown in Figure 3(e). The imaging was carried out at the tip of the Ni_xFe_{1-x} nanowire, and the results indicate that the nanowire is polycrystalline with domains of ordered structures, as shown in Figure 3(f).

For magnetic property measurement, the released $Ni_{95}Fe_5$ ($Ø = 350$ nm)/$Ni_{87}Fe_{13}$ ($Ø = 150$ nm) nanowires were dispersed on a silicon wafer and aligned by a large magnetic field of 5000 Oe. Figure 4 shows the hysteresis behaviors of the constricted cylindrical nanowires with the field applied parallel or perpendicular to the nanowire long axis, measured by alternating gradient magnetometer (AGFM). For the field applied along the long axis, the hysteresis loop gives a

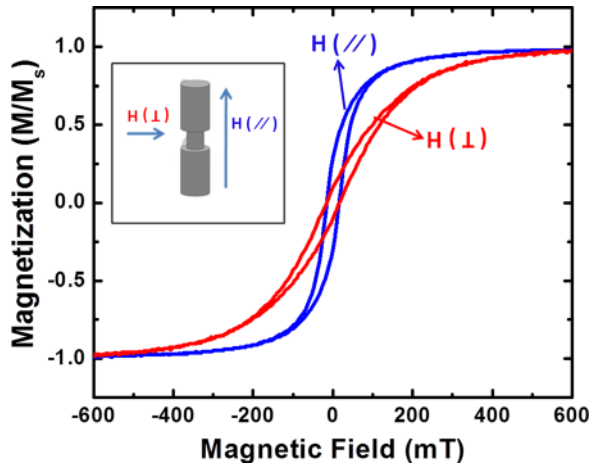

FIG. 4. Hysteresis loop measurements of the constricted $Ni_{95}Fe_5/Ni_{87}Fe_{13}$ nanowires with a magnetic field applied parallel, H (//) and perpendicular, H ($\perp$) to the nanowire axis.

remanence-to-saturation ratio $(M_r/M_s)(//)$ of 0.285. The obtained loop shape is relatively rectangular, which indicates that the easy axis is aligned along the long axis of the nanowires. When the field is applied perpendicularly to the nanowire axis, a sheared loop with a $M_r/M_s(\perp)$ ratio of 0.095 is obtained, which is a characteristic of hard-axis switching in the nanowires. The hysteresis behaviors of the non-constricted nanowire are found to be similar to that of the constricted cylindrical nanowire.

Magnetic force microscopy (MFM) scanning (Veeco Dimension 3100) was carried out on the constricted and non-constricted NiFe nanowires. A lift-scan-height of 50 nm[20] was chosen to optimize the magnetic signal. The nanowire samples were first magnetically saturated with a large external field of 5000 Oe along the nanowires long axis. The field was then removed so that the magnetization

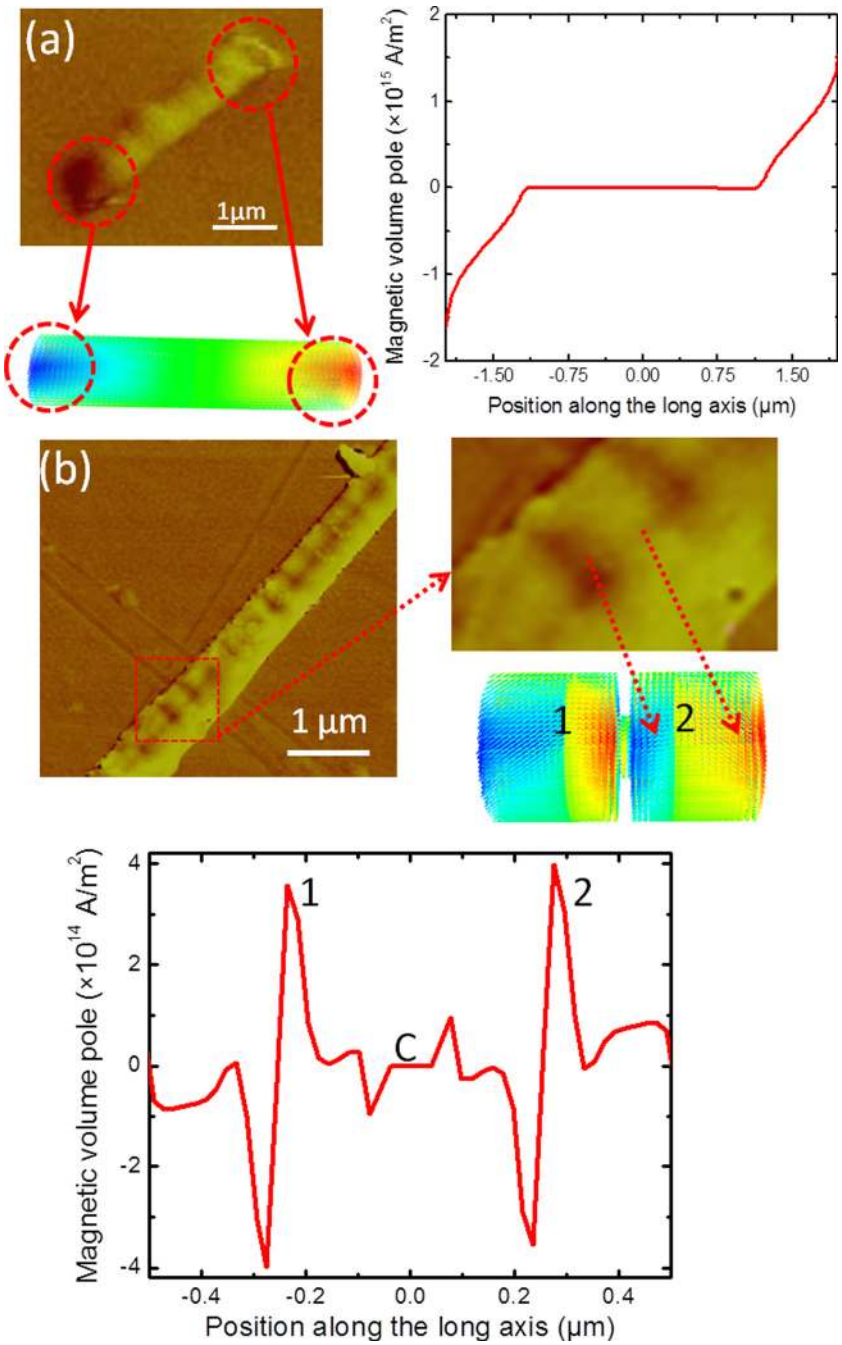

FIG. 5. (a) MFM image of the non-constricted cylindrical NiFe nanowire. Dark and bright magnetic contrasts shown at the two ends of the nanowire indicate the presence of two magnetic vortices with different chiralities. Also shown is the magnetic charge calculation along a non-constricted cylindrical nanowire. As the strength of the magnetic charges is proportional to the stray magnetic fields generated by the vortex magnetization, the magnetic charge property shown in the plot gives clear understanding of the magnetic contrast observation in the MFM image. (b) MFM image of the constricted cylindrical NiFe nanowire. The periodical bright and dark contrast spots represent the two different chirality vortices formed along the nanowire. A close-up view of the MFM image and a simulated magnetization configuration are shown for comparison. The boundary between the dark and bright spots indicates the helical DWs present in the constricted cylindrical nanowire. Shown below is the plot of magnetic charge variation at a single constriction section of along the constricted cylindrical nanowire. Helical domain walls are present at location 1 and 2, and C is the constricted region.

of the nanowires relaxed to its remanent state. Figure 5(a) shows the MFM image of the non-constricted cylindrical NiFe nanowire of diameter 250 nm. Dark and bright magnetic contrasts are observed separately at the two ends of the nanowire due to the attractive or repulsive interaction between the tip and local magnetization of the nanowire, indicating the presence of opposite magnetic charges. Also shown is the calculated magnetic charge along the 250 nm diameter cylindrical nanowire. From the plot, the magnetic charges can be ascribed to the curling of magnetization in vortex configuration with two different chiralities. The stray magnetic fields generated by clockwise or anticlockwise vortex magnetization are directly detected by the magnetic cantilever to produce the magnetic contrast. The image also reveals that the inner part of the nanowire between the two vortices has homogenous neutral contrast, and zero magnetic charge is found at the center of the nanowire which is an indication of a single-domain state. In principle, there should be no contrast at the single domain state, but the shown weak neutral contrast is attributed to the residual topographic interactions between the tip and the nanowire. Therefore, the observed MFM scanning supports the simulated magnetization configuration and the calculated magnetic charge along the non-constricted nanowire that the nanowire is composed of two vortices of opposite chirality separated by single domain state at the center.

Shown in Figure 5(b) is the MFM image of a constricted cylindrical NiFe nanowire. The image shows a series of alternate bright and dark contrast spots are present along the nanowire, which is markedly different from the magnetic image of the non-constricted nanowire. The dark and bright magnetic contrasts present in the nanowire indicate that two opposite magnetic charges present not only at the edges but also along the nanowire due to the constrictions. It reveals that clockwise and anti-clockwise vortices are present throughout the nanowire when the constrictions are introduced. Shown below the MFM image is the calculated magnetic charge of a multi-constriction cylindrical nanowire, and a single-constriction section of the calculation is plotted for analysis. In the non-constricted sections, the crossover of negative to positives magnetic charge indicates the presence of the helical domain wall, and, in this instance, it happens at location 1 and 2, as shown in the simulated magnetization diagram. The MFM scanning supports the simulation results of the formation of vortices throughout the constricted nanowires. The boundary between the dark and bright contrasts is the helical DW that connects the magnetization rotation from the anti-clockwise vortex to the clockwise vortex.

In conclusion, a three-dimensional helical domain wall had been simulated in cylindrical NiFe nanowire to connect clockwise and anti-clockwise vortex magnetizations that propagate from each end of the nanowire. The formation of such helical domain wall can be controlled by introducing constrictions with diameter less than 150 nm within the nanowire structure. We have demonstrated a technique to fabricate such constricted NiFe nanowire, and our helical domain wall micromagnetic simulations are confirmed by MFM measurements.

This work was supported in part by the NRF-CRP program (Multifunctional Spintronic Materials and Devices). We thank Zhou Tiejun (DSI, A*STAR) and Shen Yiqiang (MSE, NTU) for their assistance in experimental measurements and Sarjoosing Goolaup for useful discussion.

[1]D. A. Allwood, G. Xiong, C. C. Faulkner, D. Atkinson, D. Petit, and R. P. Cowburn, Science **309**, 1688 (2005).
[2]S. S. P. Parkin, M. Hayashi, and L. Thomas, Science **320**, 190 (2008).
[3]R. Wieser, U. Nowak, and K. D. Usadel, Phys. Rev. B **69**, 064401 (2004).
[4]R. Wieser, U. Nowak, and K. D. Usadel, Phase Trans. **78**, 115 (2005).
[5]M. Yan, A. Kakay, S. Gliga, and R. Hertel, Phys. Rev. Lett. **104**, 057201 (2010).
[6]M. Franchin, A. Knittel, M. Albert, D. S. Chernyshenko, T. Fischbacher, A. Prabhakar, and H. Fangohr, Phys. Rev. B **84**, 094409 (2011).
[7]R. Wieser, E. Y. Vedmedenko, P. Weinberger, and R. Weisendanger, Phys. Rev. B **82**, 144430 (2010).
[8]G. P. Heydon, S. R. Hoon, A. N. Farely, S. L. Tomlinson, M. S. Valera, K. Attenborough, and W. Schwarzache, J. Phys. D: Appl. Phys. **30**, 1083 (1997).
[9]R. Ferre, K. Ounadjela, J. M. Goerge, L. Piraux, and S. Dubois, Phys. Rev. B **56**, 14066 (1997).
[10]I. L. Prejbeanu, L. D. Buda, U. Ebles, M. Viret, C. Fermon, and K. Ounadjela, IEEE Trans. Mag. **37**, 2108 (2001).
[11]L. Vila, M. Darques, A. Encinas, U. Ebels, J.-M. George, G. Faini, A. Thiaville, and L. Piraux, Phys. Rev. B **79**, 172410 (2009).
[12]M. Donahue and D. G. Porter, *OOMMF User's Guide, Version 1.0, Interagency Report NISTIR 6376* (National Institute of Standard and Technology, Gaithersburg, MD, 1999).
[13]H. T. Zeng, D. Petit, L. O'Brien, D. Read, E. R. Lewis, and R. P. Cowburn, J. Magn. Magn. Mater. **322**, 2010 (2010).
[14]H. F. Liew, S. C. Low, and W. S. Lew, J. Phys.: Conf. Ser. **266**, 012058 (2011).
[15]H. P. Liang, Y. G. Guo, J. S. Hu, C. F. Zhu, L. I. Wan, and C. L. Bai, Inorg. Chem. **44**, 3013 (2005).
[16]J. J. Palfreyman, F. van Belle, W. S. Lew, T. Mitrelias, J. A. C. Bland, M. Lopalco, and M. Bradley, IEEE Trans. Magn. **43**, 2439 (2007).
[17]F. V. Belle, J. J. Palfreyman, W. S. Lew, T. Mitrelias, and J. A. C. Bland, AIP Conf. Proc. **1025**(1), 34 (2008).
[18]J. R. Choi, S. J. Oh, H. Ju, and J. Cheon, Nano Lett. **5**, 2179 (2005).
[19]P. Yong, T. Cullis, G. Mobus, X. Xu, and B. Inkson, Nanotechnology **18**, 485704 (2007).
[20]S. P. Li, W. S. Lew, J. A. C. Bland, L. Lopez-Diaz, M. Natali, C. A. F. Vaz, and Y. Chen, Nature (London) **415**, 600 (2002).